Food Chemistry: X 21 (2024) 101138

Contents lists available at ScienceDirect

Food Chemistry: X

journal homepage: www.sciencedirect.com/journal/food-chemistry-x

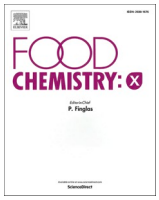

Fabrication and characterisation of collagen/pullulan ultra-thin fibers by electrospinning

Junde Chen [*,1], Jianying Li [1], Yushuang Li, Sijia Wu

Technical Innovation Center for Utilization of Marine Biological Resources, Third Institute of Oceanography, Ministry of Natural Resources, Xiamen 361005, China

ARTICLE INFO

Keywords:
Collagen
Pullulan
Electrospinning
Ultra-thin fibers
Morphology
Structure

ABSTRACT

Collagen electrospun fibers are promising materials for food packaging and tissue engineering. The conventional electrospinning of collagen, however, is usually carried out by dissolving it in organic reagents, which are toxic. In this study, collagen/pullulan (COL/PUL) ultra-thin fibers were prepared by electrospinning using acetic acid as a solvent. Compared to the conventional preparation method, the proposed method is safe and does not produce toxic solvent residues. The introduction of PUL increased the degree of molecular entanglement in the solution, so the viscosity of the COL/PUL electrospun solution increased from 0.50 ± 0.01 Pa•s to 4.40 ± 0.08 Pa•s, and the electrical conductivity decreased from 1954.00 ± 1.00 mS/cm to 1372.33 ± 0.58 mS/cm. Scanning electron microscopy analysis confirmed that PUL improved the spinnability of COL, and smooth, defect-free COL/PUL ultra-thin fibers with diameters of 215.32 ± 40.56 nm and 240.97 ± 53.93 nm were successfully prepared at a viscosity of greater than 1.18 Pa•s. As the proportion of PUL increased, intramolecular hydrogen bonds became the dominant interaction between COL and PUL. The intermolecular hydrogen bonding content decreased from 52.05 % to 36.45 %, and the intramolecular hydrogen bonding content increased from 46.11 % to 62.95 %. The COL was gradually unfolded, the content of α-helices decreased from 33.57 % to 25.91 % and the random coils increased from 34.22 % to 40.09 %. More than 36 % of the triple helix fraction of COL was retained by the COL/PUL ultra-thin fibers, whereas only 16 % of the triple helix fraction of COL was retained by the COL nanofibers prepared with 2.2.2-trifluoroethanol. These results could serve as a reference for the development of green food COL-based fibers.

1. Introduction

In recent years, studies have extensively focused on the application of biopolymers from renewable food resources due to their economic and environmental benefits, and food polymer-based nanofibers have attracted significant attention (Drosou, Krokida, & Biliaderis, 2018). This has created opportunities for food processing waste from fish, such as fish skin, scales, and bones, as these waste materials offer a rich source of natural polymer type I collagen (COL) (Jafari et al., 2020). Type I COL is a natural polymer with a stable triple helix structure, consisting of a right-handed triple superhelix structure with three α subunits (Chen et al., 2018). Due to its nonimmunogenic nature and excellent biocompatibility and biodegradability, COL has been extensively studied in the biomedical, pharmaceutical, food, and cosmetic industries. Type I COL is a major structural protein of the extracellular matrix (ECM) in organs and tissues, and plays a critical role in maintaining the biological and structural integrity of the ECM, undergoing constant remodelling for physiological functions (Blackstone, Gallentine, & Powell, 2021; Irastorza, Zarandona, Andonegi, Guerrero, & Caba, 2021). Thus, COL-based materials are now favoured in the manufacturing of biomaterials and food packaging (Ma et al., 2020).

Electrospinning has been widely used to prepare tailor-made tissue-engineered scaffolds, as the obtained fibers will have similar morphological and structural characteristics to natural ECM in tissue (Jia et al., 2021). These electrospun nanofibers exhibit excellent controllable morphology (Xiao & Lim, 2018), allowing for the simple production of continuous nanofibers with diameters in the range of sub-nanometres to micrometres, thus, mimicking the structure of natural ECM (Blackstone et al., 2021). Therefore, the electrospinning of COL into scaffolds, as a major component of native ECM, has gained increasing attention.

To manufacture COL scaffolds by electrospinning, a degree of COL denaturation is necessary for the COL to be soluble and generate a

* Corresponding author.
E-mail addresses: jdchen@tio.org.cn (J. Chen), liyushuang@tio.org.cn (Y. Li).
[1] These authors contributed equally.

https://doi.org/10.1016/j.fochx.2024.101138
Received 7 October 2023; Received in revised form 19 December 2023; Accepted 11 January 2024
Available online 16 January 2024

solution that can be electrospun (Blackstone et al., 2021). Previous studies reported that to obtain a spinnable material, the proteins must be unfolded, generating random coil structures (Rostami, Yousefi, Khezerlou, Mohammadi, & Jafari, 2019). Organic solvents, which are highly volatile and readily evaporate, have been used to facilitate the formation of COL electrospun nanofibers, such as 1,1,1,3,3,3-hexafluoro-2-propanol (HFP) (Guo et al., 2020) and 2.2.2-trifluoroethanol (TFE) (Blackstone et al., 2021). However, these solvents, are corrosive and toxic and will disrupt the natural structure of COL, causing the denaturation of COL to gelatine, resulting in gelatine nanofibers instead of COL nanofibers (Zeugolis et al., 2008; Miele et al., 2020; Li et al., 2019). Zeugolis et al. (2018) reported that electrospinning COL using fluoroalcohols caused damage to the α-chains, and the triple helix and fibrillar structure was disrupted, with a lack of internal structure or configuration order similar to those obtained from gelatine preparation. Liu, Teng, Chan & Chew (2010) reported that only 12.51 % of the triple helix fraction of COL was retained using HFP. Fiorani et al. (2014) also reported that the use of TFE electrospun COL nanofibers as a solvent resulted in only 16 % of the triple helix fraction being retained. Furthermore, although the toxic solvents will evaporate during the spinning process, their residues may affect subsequent applications. Therefore, using environmentally friendly and benign solvent systems for electrospinning is critical for retaining the triple helix structure of COL and subsequent application of the nanofibers. This serves as a good opportunity for acetic acid, which has previously been encouraged by EU regulations for use as a green solvent instead of toxic or hazardous solvents (Miele et al., 2020). Acetic acid is an environmentally friendly and nontoxic solvent that is generally recognised as safe (GRAS), and can be obtained from cellulosic biomass such as agricultural residue. Therefore, using acetic acid as a solvent may help facilitate the development of inexpensive and renewable raw materials (Miele et al., 2020; Rostami et al., 2019). Acetic acid is a frequently used solvent for electrospinning, and it has a positive impact on the preparation of nanofibers. Stie, Jones, Sorensen, Jacobsen, Chronakis & Nielsen (2019) demonstrated that using acetic acid as a solvent produced chitosan/polyethylene oxide nanofibers that could be maintained in water for 4 h and still retain their shape and fibrous structure, whereas the use of succinic or citric acid as solvents resulted in the disintegration of chitosan/polyethylene oxide nanofibers mats after 4 h in water. Han, Youk, Min, Kang & Park (2008) were the first to prepare long and homogeneous cellulose acetate (CA) nanofibers by using a solvent mixture of acetic acid/water, and they showed that increasing the proportion of acetic acid in the solvent mixture increased the diameter of CA nanofibers. Vu, Morozkina, Uspenskaya & Olekhnovich (2022) showed that the use of acetic acid as a solvent had no effect on the chemical properties of the prepared polyvinyl alcohol (PVA) nanofibers, and the mechanical strength of the PVA nanofibers increased with the concentration of acetic acid in the electrospun solution. Thus, acetic acid can be used as a solvent for dispersing COL for the manufacture of COL-based fibers.

Pullulan (PUL), a microbial and linear polysaccharide, is primarily composed of repeating α-(1/6)-linked maltotriose units. PUL, a polysaccharide on the GRAS list, can also be used as a spinning material (Jia, Qin, Xu, Kong, Liu, & Wang, 2020). PUL also has the ability to form hydrogen bonds with proteins, and during the electrospinning process, it can improve the spinnability of proteins by changing the properties of the polymer solutions by binding to the proteins through hydrogen bonds (Jia et al., 2020).

Therefore, in this work, we prepared fish COL/PUL ultra-thin fibers by electrospinning using acetic acid as a solvent. According to our hypothesis, the introduction of PUL would improve the spinnability of the electrospun solution by forming hydrogen bonds with the COL. The interaction (hydrogen bonding) between COL and PUL molecules and the change in secondary structure conformation underlying the increased spinnability of COL were investigated. The structure and properties of COL/PUL ultra-thin fibers were also characterised.

2. Materials and methods

2.1. Materials

Red stingray (*Dasyatis akajei)* skin was purchased from an aquatic product processing plant located in Zhangzhou, China, and the protein markers (26634) were purchased from Thermo Fisher Scientific Baltics (Vilnius, Lithuania). PUL with a purity of 99 % was purchased from Solarbio Science & Technology Co., Ltd. (Beijing, China). All chemical reagents used in this study were of analytical grade.

2.2. Preparation of COL from red stingray skin

COL from red stingray skin was prepared according to the procedures reported by Chen et al. (2018), with slight modifications. All procedures were performed at 4 °C. The red stingray skin was soaked with 0.5 M acetic acid (1:20 w/v) for 12 h under stirring (Eurostar 20 digital, IKA, Staufen, Germany), followed by centrifugation at 9000 rpm for 30 min at 4 °C. Sodium chloride (NaCl) was then added to the supernatant to bring the final concentration of COL to 5 % (w/v). After 1 h, the precipitate was collected by centrifugation at 9000 rpm for 30 min at 4 °C, and the resultant precipitate was redissolved in 0.5 M acetic acid at a ratio of 1:15 (w/v). The solution obtained was then dialysed against 0.1 M acetic acid for 1 day, followed by dialysis against distilled water for 2 days.

2.3. Sodium dodecyl sulphate–polyacrylamide gel electrophoresis (SDS-PAGE)

We performed SDS-PAGE on a mini-protein vertical slab electrophoresis system (Bio-Rad Laboratories, Hercules, CA, USA), with a buffer of 0.025 M Tris-HCl (pH of 8.3, including 0.192 M glycine and 0.1 % w/w SDS) (Laemmli, 1970). COL (1 mg/mL) was dissolved in distilled water and thoroughly mixed with a sample loading buffer (277.8 mM Tris-HCl, pH 6.8, 44.4 % (v/v) glycerol, 4.4 % SDS and 0.02 % bromophenol blue) at a 4:1 (v/v) ratio. The solution was then heated at 100 °C for 3 min. Subsequently, 8 μL of each sample solution was loaded onto a gel consisting of 7.5 % separating gel and 4.5 % stacking gel. Electrophoresis was run for 80 min at a constant voltage of 110 V at room temperature, followed by soaking in 50 % (v/v) methanol and 10 % (v/v) acetic acid. Staining was then conducted with 0.125 % Coomassie Brilliant Blue R-250 in 50 % (v/v) ethanol and 10 % (v/v) acetic acid, and finally destained with 50 % (v/v) ethanol and 10 % (v/v) acetic acid. The molecular weight of the samples was estimated by using protein markers (26634), using Quantity One 4.6.0 software (Bio-Rad Laboratories).

2.4. Preparation of the electrospun solutions

COL (10 %, 15 %, 20 % and 25 %, w/v) was dissolved in 0.4 M acetic acid under stirring (RCT digital, IKA) for 2 h at room temperature (22–25 °C). The concentration of COL in the composite system was determined by testing the spinnability of different COL concentrations.

PUL was added to the COL solution at different proportions, with COL:PUL at 1:0.5, 1:0.75, 1:1, 1:1.25, 1:1.5, and 1:1.75 (w/w) at determined previously COL concentrations. The composite solutions were stirred for 12 h at room temperature (22–25 °C) to ensure the complete solubilisation of COL and PUL before the electrospinning process.

2.5. Electrospinning process

The electrospun solutions were placed into a syringe at 20 kV voltage (Dongwen High Voltage Power Supply Co., Ltd., Tianjin, China) with a flow rate of 0.1 mL/h. The distance between the needle and the collector was 15 cm, and aluminium foil was used to collect the fibers. The

experiments were conducted at 22 ± 2 °C and a relative humidity of 40 ± 5 %. The COL ultra-thin fibers (10 %, 15 %, 20 %, and 25 %, w/v) were denoted as C1, *C*2, C3, and C4, respectively, while the COL/PUL ultra-thin fibers (COL:PUL at 1:0.5, 1:0.75, 1:1, 1:1.25, 1:1.5, and 1:1.75, w/w) were denoted as CP1, CP2, CP3, CP4, CP5, and CP6, respectively. The sample was stored in a desiccator at room temperature (22 ± 2 °C) until further analysis.

2.6. Morphology

The morphology of the samples was investigated by a Quanta scanning electron microscope (SEM) (Quanta 450FEG, FEI, Waltham, MA, USA). The samples were glued on the sample table of the SEM with conductive tape, and the samples were observed under an accelerating voltage of 10 kV after they were sputter-coated with gold. The average fiber diameters were calculated by measuring 100 randomly selected data points in each SEM image containing 100 fibers, using ImageJ 1.8.0 software (National Institute of Mental Health, Bethesda, MD, USA) and SEM images obtained at a magnification of 16000 ×.

2.7. Characterisation of the electrospun solutions

2.7.1. Viscosity

The viscosity of the sample solutions was measured by a rotational rheometer (MCR 302, Anton Paar, Austria) with a stainless-steel cone/plate geometry (0.5° cone angle, 60-mm cone diameter). The gap was 57 μm and the temperature was 25 °C (Mohammadi, Ramazani, Rostami, Raeisi, Tabibiazar, & Ghorbani, 2019). The shear rate was increased from 0.1 to 1000 s^{-1}, and the viscosity of the sample solutions was recorded at 100 s^{-1}. The flow behaviours of the solutions were analysed as follows (Xiao et al., 2018):

$$\sigma = K\gamma^{n} \tag{1}$$

where σ is the shear stress (Pa), K is the consistency index (Pa·s^{n}), γ is the shear rate (s^{-1}), and n is the flow behaviour index (dimensionless).

The apparent viscosity of the electrospun solution was calculated as follows:

$$\eta = K\gamma^{n-1} \tag{2}$$

where η is the apparent viscosity (Pa·s).

2.7.2. Electrical conductivity

The electrical conductivity of the sample solutions was measured by a conductivity meter (Seven2Go, METTLER TOLEDO, Switzerland) at room temperature (22–25 °C). First, 5 mL of sample solution was transferred to a 15-mL centrifuge tube. Then, the probe was submerged in the sample solution until the sensor was covered and the measured values stabilised.

2.7.3. Surface tension

The surface tension of the sample solutions was measured by the Wilhelmy plate method using a tensiometer (DCAT21, Dataphysics, Filderstadt, Germany) at room temperature (22–25 °C), referring to Mouzouvi, Umerska, Bigot & Saulnier (2017) and Manning-Benson, Bain, Darton, Sharpe, Eastoe & Reynolds (1997) with slight modifications. We placed 15 mL of each sample into a 20 mL crystalline dish with a platinum sheet (PT 9, length 10 mm, width 9.95 mm, thickness 0.2 mm) submerged to a depth of 3 mm, and raised the platinum sheet at a rate of 1.0 mm/s until it was completely removed from the surface of the sample solution. During this process, 50 consecutive measurements were taken automatically until the standard deviation of the surface tension value was less than 0.03 mN/m. The test was stopped and the surface tension value was recorded. The platinum sheet was then carefully cleaned with anhydrous ethanol and dried with an alcohol lamp between measurements.

2.8. Fourier-transform infrared spectroscopy (FT-IR) analysis

FT-IR analysis was conducted to study the possible inter- and intramolecular interactions and changes of secondary structural conformation between COL and PUL. The samples obtained from electrospinning were mixed with KBr by grinding at the ratio of 1:100 (w/w), and then investigated by using a spectrophotometer (VERTEX 70, Bruker, Karlsruhe, Germany) within the wavelength range of 4000–400 cm^{-1} at a resolution of 4 cm^{-1}. The –OH stretching region (3800–3000 cm^{-1}) and amide I band (1700–1600 cm^{-1}) were smoothed every 7 points using the Savitzky-Golay method, followed by second derivative analysis (OMNIC8.2 software, Thermo Nicolet, USA). The final fitted curves were subsequently obtained by Gaussian curve-fitting (PeakFit v4.12 software, SPSS Inc., Chicago, IL, USA).

2.9. Circular dichroism (CD)

The freeze-dried collagen (FDC), denatured collagen (DNC), and CP1–6 were dissolved in 0.1 mg/mL of 0.1 M acetic acid and equilibrated for 24 h at 4 °C. The DNC was obtained by heating the FDC at 95 °C for 3 h. Each sample was centrifuged at 10000 × *g* for 10 min at 4 °C (Neofuge 15R, Shanghai Lishen Scientific Equipment Co., Ltd., China), and the supernatants were measured by a CD spectropolarimeter (Chirascan, Applied Photophysics Ltd., UK) with a path length of 0.1 mm. The CD spectra of the samples were recorded at wavelengths of 190–300 nm at room temperature at a scanning speed of 20 nm/min. The spectrum of the 0.5 M acetic acid was used as the baseline and each sample spectrum was determined according to the average results of three tests. The triple helical fraction of the sample was calculated as follows (Fiorani et al., 2014):

$$f_{TH} = \frac{[\theta]_{CP} - [\theta]_{DNC}}{[\theta]_{FDC} - [\theta]_{DNC}} \times 100 \tag{3}$$

where f_{TH} denotes the fraction triple helices in the sample measured at wavelength λ (%), $[\theta]_{CP}$ is the ellipticity of CP1–6 at wavelength λ (deg·cm^2·mol^{-1}), $[\theta]_{DNC}$ is the ellipticity of denatured collagen at wavelength λ (deg·cm^2·mol^{-1}), and $[\theta]_{FDC}$ is the ellipticity of FDC at wavelength λ (deg·cm^2·mol^{-1}).

2.10. Mechanical properties

The tensile strength of the samples was measured by a tensile tester (XQ-1C, Shanghai New Fiber Instrument Co., Ltd., Shanghai, China). All samples were collected on aluminium foil and then were cut into specimens with dimensions of 20 mm × 5 mm (length × width). Each sample was operated at a strain rate of 20 mm/min for testing, in the temperature range of 22–25 °C and at a relative humidity of 40 %, with each sample measured three times.

2.11. Thermal stability

The thermal stability of the samples was measured by a thermogravimetric analyser (TGA) (TGA3, METTLER TOLEDO, Switzerland). Sample measurements were obtained at 50 mL/min under an N_2 atmosphere and heated from 30 °C to 600 °C at a constant heating rate of 10 °C/min.

2.12. Porosity

The porosity of the samples was calculated from the raw SEM images using ImageJ 1.8.0 software, according to the methods described by Tort, Acartürk & Besikci (2017). The ultra-thin fibers were coloured in black and the pores were coloured in white using ImageJ software, and the areas of the two colours were calculated by ImageJ software. The percentage of pores relative to the total surface area in each image was

defined as the porosity (%).

2.13. Statistical analysis

We performed analysis of variance (ANOVA) using SPSS Version 17.0 software (IBM SPSS Statistics, Ehningen, Germany), with different letters indicating significant differences in ultra-thin fiber diameters between the samples ($p < 0.05$). All experiments were performed in triplicate and the results were expressed as mean ± standard deviation (SD).

3. Results and discussion

3.1. SDS-PAGE

The SDS-PAGE results of the COL from the red stingray skin are shown in Fig. 1. Type I COL from rat tail was used as the standard. The red stingray skin COL and type I COL had similar protein patterns, and both consisted of two different types of α-chains (α1 and α2), where the molecular weights of the α1-chains and α2-chains were approximately 130 kDa and 120 kDa, respectively. High-molecular-weight components were observed, including dimeric β-chains with molecular weights of approximately 200 kDa, and a small quantity of trimeric γ-chains with molecular weights of approximately 250 kDa. Moreover, the ratio of α1-chains and α2-chains was approximately 2:1, suggesting that the COL isolated from red stingray skin could be characterised as type I COL ($[\alpha1]_2\alpha2$) (Chen et al., 2018).

3.2. Spinnability of the COL solutions

In this study, we tested the spinning properties of different concentrations of fish COL solutions. The morphologies of the ultra-thin fibers obtained from different concentrations of COL electrospun solutions are shown in Fig. 2. Because the entanglement of the molecules in the COL solution was not sufficient to produce defect-free fibers, we obtained bead fibers at 10 %–20 % (w/v) COL concentration (Fig. 2 C1–3) (Drosou et al., 2018). When the COL concentration was increased to 25 % (w/v), the electrospun solution could not form a Taylor cone at the tip of the needle, preventing it from spinning. As shown in Fig. S1, the electrospun solution adhered to the needle tip and was stretched in the electrostatic field. Subsequently, the electrospun solution dripped onto the aluminium foil under the electrostatic field.

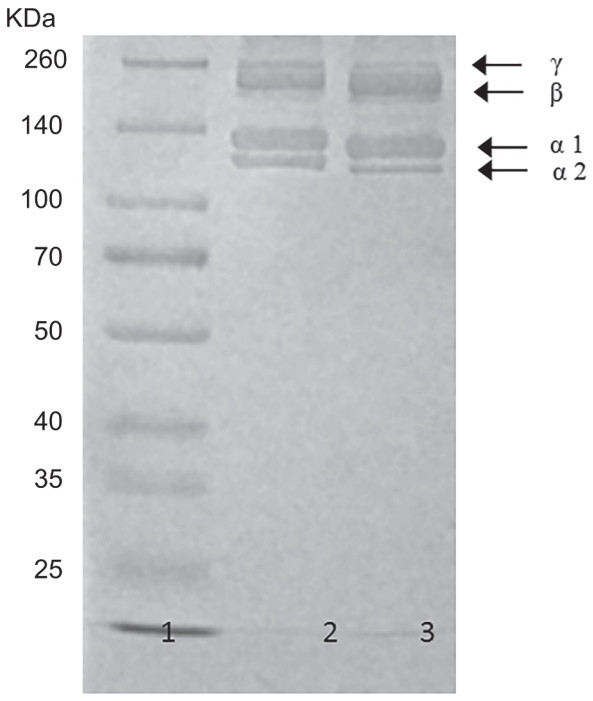

Fig. 1. SDS-PAGE pattern. (1) protein marker; (2) rat tail collagen; (3) red stingray skin collagen.

The above results indicated that the spinning properties of COL solutions were inadequate, and molecular entanglement in the COL solutions was insufficient to produce defect-free fibers during the electrospinning process. As determined by Drosou et al. (2018), insufficient spinning properties of solutions or polymers could result in bead fiber formation. Therefore, we improved the spinning properties of the COL solutions by increasing the degree of entanglement in the solutions by introducing PUL. PUL and COL were blended at different ratios to prepare electrospun solutions in the following experiments, according to a COL concentration of 10 % (w/v).

3.3. Effect of COL/PUL solution ratio on ultra-thin fibers

The viscosity, electrical conductivity, and surface tension of the electrospun solutions played a crucial role in the electrospinning process, and these physicochemical properties considerably defined the morphology and size of the nanofibers (Colín-Orozco, Zapata-Torres, Rodríguez-Gattorno, & Pedroza-Isla, 2015). The physicochemical properties of COL/PUL electrospun solution and power law parameters from the shear thinning properties are shown in Table 1. The flow curves of the COL/PUL solutions are shown in Fig. S2, indicating that all curves obeyed the power law (Jia et al., 2020). Viscosity, which affected the degree of entanglement of the electrospun solutions, increased from 0.50 ± 0.01 to 4.40 ± 0.08 Pa·s ($p < 0.05$) at 100 Hz as the ratio of PUL in COL/PUL increased from 1:0.5 (w/w) to 1:1.75 (w/w). In addition, the viscosity decreased with increasing shear rate, suggesting that the solutions exhibited the shear thinning behaviour of a non-Newtonian fluid (Jia et al., 2020; Xiao et al., 2018). These phenomena are also shown in Table 1, where the consistency index K was related to the viscosity of the solution at low shear rates, which increased with increasing PUL content ($p < 0.05$) (Kutzli, Gibis, Baier, & Weiss, 2019). All n values were less than 1 (0.79–0.85), indicating that the COL/PUL solutions were shear-thinning fluids. Shear thinning behaviour is usually associated with polymer entanglement, which is a prerequisite for fiber formation during electrospinning (Kutzli et al., 2019). Therefore, the increase in K and shear thinning behaviour of the solution indicated the presence of chain-chain interactions (hydrogen bonding) between the COL and PUL molecules, which caused the degree of entanglement in the solution to increase (Jia et al., 2020; Xiao et al., 2018). We also found that the changes in COL/PUL ratio had a very slight effect on the surface tension of the electrospun solutions (44.11–46.14 mN/m) (Table 1), indicating that the surface tension was not the main factor affecting solution spinnability and ultra-thin fiber morphology in this experiment. Moreover, we observed that the electrical conductivity of electrospun solutions decreased from 1954.00 ± 1.00 to 1372.33 ± 0.58 mS/cm as the ratio of PUL in COL/PUL increased from 1:0.5 to 1:1.75 (w/w). The electrical conductivity showed a significant decrease ($p < 0.05$) with increasing PUL content, which was similar to the phenomenon reported by Jia et al. (2020). This could be due to the interaction between the amino group of the protein and the hydroxyl group of the polysaccharides, resulting in a decrease in the electrical conductivity of the solution. As the amount of PUL in the solution increased, the interaction between COL and PUL became more intense, resulting in a rapid decrease in electrical conductivity. This decrease in electrical conductivity is beneficial for electrospinning (Aceituno-Medina, Mendoza, Lagaron, & Lopez-Rubio, 2013).

SEM images of the ultra-thin fibers were obtained for various COL/PUL solutions, and the histograms of the ultra-thin fibers diameter distributions are shown in Fig. 3. Noticeably, the introduction of PUL led to significant changes in ultra-thin fiber morphology, with the disappearance of bead fibers, and morphological conversion of the fibers from

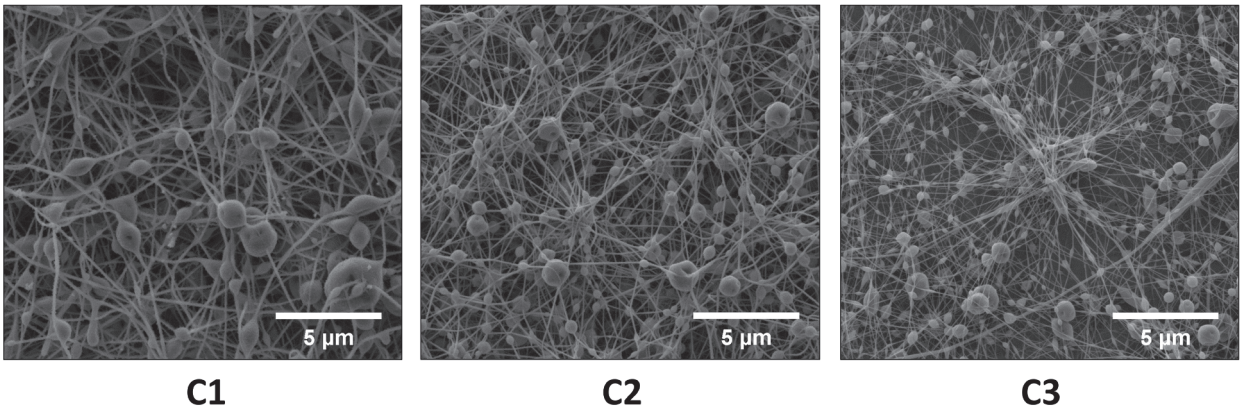

Fig. 2. SEM micrographs of (C1–3) ultra-thin fibers at 16000 × magnification.

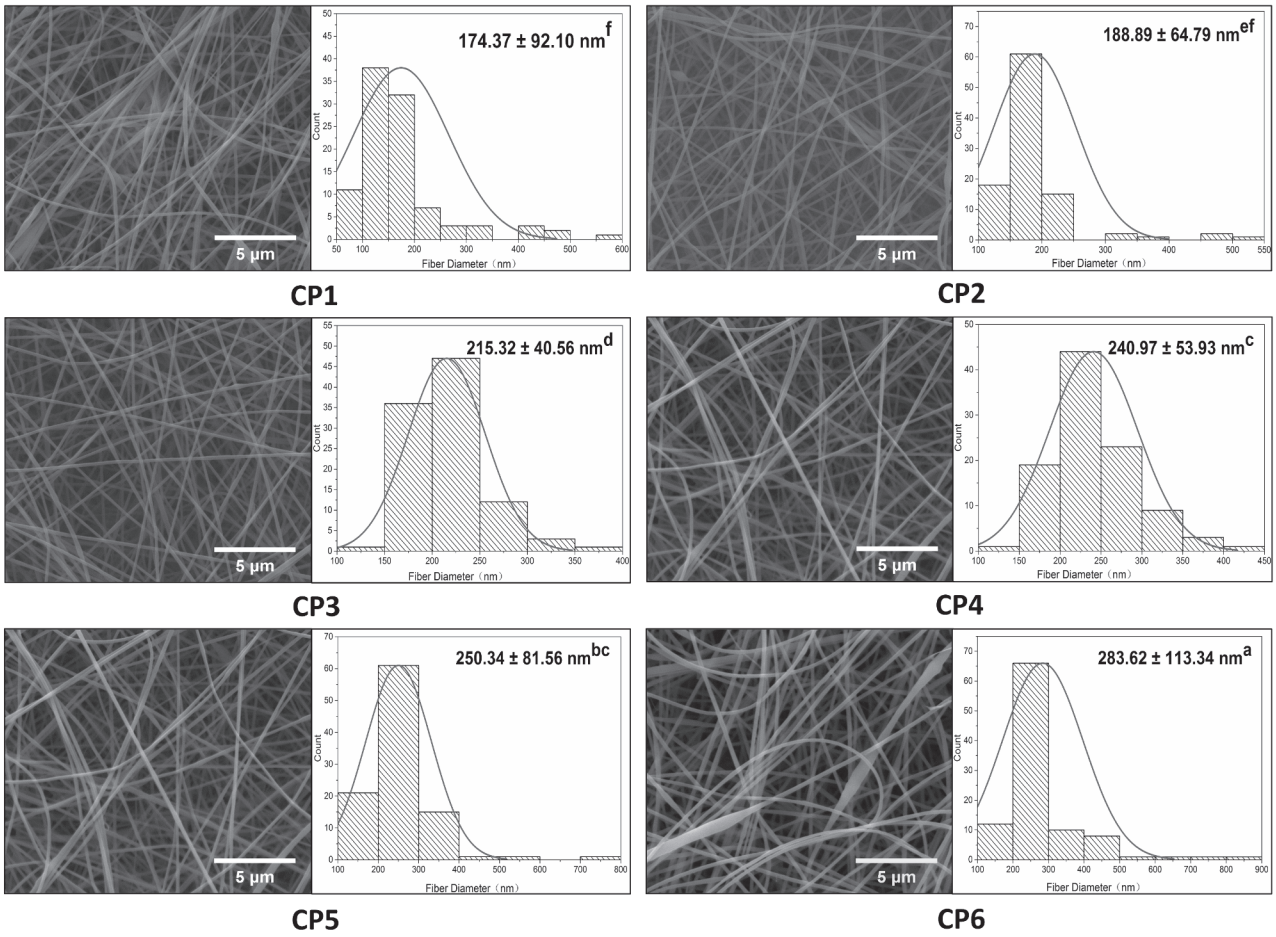

Fig. 3. SEM micrographs of (CP1–6) ultra-thin fibers at 16000 × magnification and the corresponding histogram of the diameter distribution.

spindle-like to continuous and smooth, and back to spindle-like again. With the initial introduction of PUL, the ultra-thin fiber morphology changed from bead fibers (Fig. 2 C1) to spindle-like fibers (Fig. 3 CP1), and the average diameter of CP1 was 174.37 ± 92.10 nm, with a distribution ranging from 50 to 600 nm. As the ratio of PUL in COL/PUL increased to 1:0.75 (w/w), the spindle-like fibers decreased in CP2, with an average fiber diameter of 188.89 ± 64.79 nm and a distribution of 100–550 nm. These results indicated insufficient entanglement between COL and PUL to produce defect-free fibers in the COL/PUL electrospun solutions with viscosities of 0.50 and 0.90 Pa•s. Continuous and smooth ultra-thin fibers (Fig. 3 CP3–4) were obtained from COL/PUL electrospun solutions with ratios of 1:1 and 1:1.25 (w/w), indicating that when the viscosity of the COL/PUL electrospun solution reached 1.18 Pa•s, sufficient intermolecular entanglement occurred to prevent the fiber jet from breaking up into droplets, resulting in defect-free fibers (Bhattarai, Bachu, Boddu & Bhaduri, 2019). The average diameters of CP3 and CP4 were 215.32 ± 40.56 and 240.97 ± 53.93 nm, respectively. Due to the smooth fibers, CP3 and CP4 exhibited narrow fiber diameter distributions compared to CP1 and CP2, and were mainly distributed in the ranges of 150–250 nm and 150–300 nm, respectively. The increase in

Table 1
Viscosity, surface tension, electrical conductivity, power law parameters from the shear thinning properties, and morphology of ultra-thin fibers of different ratio COL/PUL blended solutions.

COL:PUL	Viscosity (Pa·s)	Surface tension (mN/m)	Electrical conductivity (mS/cm)	Consistency index, *K*	Flow behavior index, n	Morphology
1:0.5	0.50 ± 0.01^{f}	46.14 ± 0.15^{a}	1954.00 ± 1.00^{a}	1.17 ± 0.06^{f}	0.82 ± 0.01^{bc}	Fibers and spindles
1:0.75	0.90 ± 0.05^{e}	45.54 ± 0.52^{b}	1826.33 ± 1.15^{b}	2.10 ± 0.16^{e}	0.83 ± 0.01^{b}	Fibers and several spindles
1:1	1.18 ± 0.03^{d}	44.11 ± 0.05^{b}	1610.00 ± 1.73^{c}	2.51 ± 0.09^{d}	0.85 ± 0.00^{a}	Fibers
1:1.25	2.00 ± 0.06^{c}	44.71 ± 0.40^{b}	1527.00 ± 0.00^{d}	4.18 ± 0.13^{c}	0.84 ± 0.00^{a}	Fibers
1:1.5	3.58 ± 0.11^{b}	44.80 ± 0.82^{b}	1491.33 ± 1.53^{e}	8.66 ± 0.19^{b}	0.82 ± 0.01^{c}	Fibers and several spindles
1:1.75	4.40 ± 0.08^{a}	45.33 ± 0.26^{ab}	1372.33 ± 0.58^{f}	13.34 ± 0.24^{a}	0.79 ± 0.00^{d}	Fibers and several spindles

Results expressed as the mean ± standard deviation of at three independent experiments. Different letters (a-f) indicate significant ($p < 0.05$) differences between samples.

average diameter ($p < 0.05$) of the ultra-thin fibers was the combined result of viscosity and electrical conductivity in the electrospun solution, and smooth fibers were obtained. The increase in the PUL ratio resulted in more entanglements between the COL and PUL molecules, which led to an increase in the viscosity of the solution. This increase in the viscosity of the solution led to an increase in the average diameter of the ultra-thin fibers (Horuz & Belibagli, 2018). Moreover, the decrease in electrical conductivity led to a compact electrified Taylor cone plume, which also increased the average nanofiber diameter (Wang et al., 2014). However, spindle-like fibers appeared again with a further increase in the ratio of PUL in COL/PUL (1:1.5–1:1.75, w/w). The average diameters of CP5 and CP6 were 250.34 ± 81.56 and 283.62 ± 113.34 nm, respectively, and the reappearance of spindle-like fibers caused a larger average diameter and broader fiber diameter distribution (Fig. 3 CP5–6). This could be attributed to the higher viscosity (3.58 ± 0.11 and 4.40 ± 0.08 Pa•s) and lower electrical conductivity (1491.33 ± 1.53 and 1372.33 ± 0.58 mS/cm), leading to the delayed formation of Taylor cones and reducing the deformability of the jets (Kutzli et al., 2019), yielding spindle-like fibers instead of smooth ultra-thin fibers.

The above results showed that the entanglement of molecules in the electrospun solution was improved by the addition of PUL, which was beneficial for improving the spinning properties of COL. The viscosity of the solution was positively correlated with the degree of entanglement between COL and PUL molecules, and the degree of entanglement of COL and PUL molecules might be an important factor affecting the morphology of the ultra-thin fibers. Additionally, the diameter of the ultra-thin fibers was affected by a combination of the viscosity and electrical conductivity of the solution. The increased viscosity and decreased electrical conductivity of the COL/PUL electrospun solution was favourable for the formation of smooth and defect-free fibers.

3.4. Effect of the COL/PUL ratio on the vibrational bands of COL/PUL ultra-thin fibers

The FT-IR spectra of the COL, PUL, and COL/PUL ultra-thin fibers are shown in Fig. S3. In the COL spectrum, five characteristic peaks of COL were observed, with absorption peaks located at 3323 cm^{-1} (N—H stretching vibrations), 2919 cm^{-1} (asymmetrical stretch of C—H), 1660 cm^{-1} (C═O stretching), 1542 cm^{-1} (N—H bending vibration), and 1238 cm^{-1} (N—H deformation and C—N stretching) as the characteristic bands of amide A, amide B, amide I, amide II, and amide III, respectively (Chen et al., 2018). Amide I band serves as a sensitive marker of protein, providing information regarding the secondary polypeptide chains, and can be used to analyse secondary structures. We observed a slight shift in amide I band in Fig. S3, which could be attributed to PUL altering the secondary structure of COL. Five typical characteristic bands of COL were also observed in the CP1–6 spectrum. A broad absorption band was observed between 3000 and 3800 cm^{-1}, which was related to the N—H stretching vibration of the amide A band and O—H stretching of pullulan, and was affected by inter- or intramolecular hydrogen bonding (Drosou et al., 2018; Jia et al., 2020). We found that when the ratio of PUL in COL/PUL was increased from 1:0.5 (w/w) to 1:1.75 (w/w), the broad absorption bands near 3300 cm^{-1} exhibited blueshift, which were observed at 3339.96 cm^{-1}, 3348.81 cm^{-1}, 3368.04 cm^{-1}, 3389.23 cm^{-1}, 3393.04 cm^{-1} and 3419.00 cm^{-1}, respectively. This suggested that hydrogen bonding between the –NH group of COL and the –OH group of PUL may have played a role in the peak shift (Drosou et al., 2018). Other features of pullulan were also observed in the spectrum, including an absorption band located around 2931 cm^{-1}, which was associated with C—H stretching. In addition, a typical pullulan absorption band originating from the α-glucopyranosyl units was observed at 851 cm^{-1}, and the absorption bands caused by two major bonds of pullulan (α-(1,4) glycosidic bonds and α-(1,6) glycosidic bonds were found near 759 cm^{-1} and 930 cm^{-1} (Aceituno-Medina et al., 2013). The above results demonstrated that the blending of COL and PUL efficiently occurred in CP1–6 obtained by electrospinning.

To investigate the interactions between the COL and PUL molecules and possible secondary structure changes in the COL/PUL ultra-thin fibers, Gaussian curve-fitting was carried out on the –OH stretching region (3800–3000 cm^{-1}) and amide I band (1700–1600 cm^{-1}), with $R^2 > 0.999$ for all curves.

3.4.1. –OH stretching region (3800–3000 cm^{-1})

The fitted curves obtained for the –OH stretching region (3800–3000 cm^{-1}) of the ultra-thin fibers with different COL/PUL ratios are shown in Fig. S4, and their corresponding hydrogen bond types and relative absorption strengths are presented in Table 2, according to Zhang, Guo, Liu, Chen, Zhang & Yu (2018). We observed that both spectra consisted of six absorption peaks that could be classified as nonhydrogen bonds (–OH) and intra- and intermolecular hydrogen bonds. In addition, OH···OH played a dominant role in the intramolecular hydrogen bonds, and OH···ether O predominated in the intermolecular hydrogen bonds in the COL/PUL systems. As shown in Fig. 4A, when the ratio of PUL in COL/PUL increased from 1:0.5 to 1:1.75 (w/w), the content of the free-hydroxyl groups gradually decreased from 1.84 % to 0.60 % ($p < 0.05$). Furthermore, the content of intermolecular hydrogen bonds decreased from 52.05 % to 36.45 % (Fig. 4C), while the intramolecular hydrogen bonds increased from 46.11 % to 62.95 % ($p < 0.05$) (Fig. 4B). The changes in hydrogen bonding type in the COL/PUL system indicated that PUL primarily reacted with the groups forming intermolecular hydrogen bonds, as the PUL content increased. In addition, during this process, most of the free hydroxyl groups and intermolecular hydrogen bonds were broken (Mobika, Rajkumar, Sibi, & Priya, 2021) and converted to intramolecular hydrogen bonds, causing the intramolecular hydrogen bonds to become the dominant type of hydrogen bonding between COL and PUL in the COL/PUL systems.

3.4.2. Amide I band (1700–1600 cm^{-1})

We analysed the secondary structure conformational changes of the COL/PUL system according to the amide I band (1700–1600 cm^{-1}) (Liu, Wang, Sulemaan, Shen, & Zhang, 2019). The fitted curves are shown in Fig. S5, and different types of secondary structural conformations and their corresponding contents are shown in Fig. 4D. The fitted curves

Table 2
Types and relative strength of hydrogen bonds of COL/PUL ultra-thin fibers obtained from –OH stretching region (3800–3000 cm^{-1}).

Sample	Type of hydrogen bond	Abbreviation	Wavenumber (cm^{-1})	Relative strength (%)	
CP1	Free hydroxyl	I -OH	3611	1.84 ±0.03	1.84 ±0.03
	Intramolecular hydrogen bonds	II OH···OH	3434	36.64 ±0.13	46.11 ±0.21
		III Annular polymer	3177	9.47 ±0.08	
	Intermolecular hydrogen bonds	IV OH···π	3542	11.41 ±0.11	52.05 ±0.43
		V OH···ether O	3296	38.25 ±0.30	
		VI OH···N	3075	2.39 ±0.02	
CP2	Free hydroxyl	I -OH	3616	1.48 ±0.06	1.48 ±0.06
	Intramolecular hydrogen bonds	II OH···OH	3436	39.48 ±0.18	48.05 ±0.21
		III Annular polymer	3173	8.57 ±0.03	
	Intermolecular hydrogen bonds	IV OH···π	3549	11.23 ±0.05	50.47 ±0.23
		V OH···ether O	3291	37.12 ±0.18	
		VI OH···N	3076	2.12 ±0.01	
CP3	Free hydroxyl	I -OH	3616	1.02 ±0.16	1.02 ±0.16
	Intramolecular hydrogen bonds	II OH···OH	3434	43.26 ±0.39	50.65 ±0.43
		III Annular polymer	3171	7.39 ±0.03	
	Intermolecular hydrogen bonds	IV OH···π	3550	10.55 ±0.06	48.33 ±0.33
		V OH···ether O	3286	35.98 ±0.28	
		VI OH···N	3076	1.8 ±0.01	
CP4	Free hydroxyl	I -OH	3617	0.82 ±0.26	0.82 ±0.26
	Intramolecular hydrogen bonds	II OH···OH	3432	47.38 ±1.36	54.38 ±1.47
		III Annular polymer	3168	7.00 ±0.11	
	Intermolecular hydrogen bonds	IV OH···π	3553	10.67 ±0.39	44.8 ±1.21
		V OH···ether O	3280	32.46 ±0.81	
		VI OH···N	3078	1.67 ±0.02	
CP5	Free hydroxyl	I -OH	3612	0.78 ±0.08	0.78 ±0.08
	Intramolecular hydrogen bonds	II OH···OH	3434	53.17 ±1.07	58.6 ±2.02
		III Annular polymer	3160	5.43 ±0.96	
	Intermolecular hydrogen bonds	IV OH···π	3553	8.49 ±0.54	40.62 ±1.30
		V OH···ether O	3268	30.75 ±0.57	
		VI OH···N	3076	1.38 ±0.19	
CP6	Free hydroxyl	I -OH	3592	0.60 ±0.13	0.6 ±0.13
	Intramolecular hydrogen bonds	II OH···OH	3416	59.39 ±2.31	62.95 ±3.64
		III Annular polymer	3159	3.56 ±1.34	
	Intermolecular hydrogen bonds	IV OH···π	3539	7.97 ±1.53	36.45 ±2.8
		V OH···ether O	3260	27.71 ±0.65	
		VI OH···N	3077	0.77 ±0.63	

obtained from COL/PUL consisted mainly of eight subpeaks, including conformation α-helices (1646–1664 cm^{-1}), β-sheets (low band 1615–1637 cm^{-1} and high band 1682–1700 cm^{-1}), β-turns (1664–1681 cm^{-1}), and random coils (1637–1645 cm^{-1}) (Liu et al., 2019). As shown in Fig. 4D, as the ratio of PUL in COL/PUL increased from 1:0.5 to 1:1.75 (w/w), the content of α-helices decreased from 33.57 % to 25.91 % and the content of β-turns decreased from 13.21 % to 7.40 % ($p < 0.05$). In addition, the β-sheets and random coils increased from 19.00 % to 26.6 %, and from 34.22 % to 40.09 %, respectively ($p < 0.05$). The changes in conformation of the secondary structure in the COL/PUL system indicated molecular interactions (hydrogen bonding) between COL and PUL, favouring the transition of α-helices and β-turns to β-sheets and random coil structures. Furthermore, previous studies reported that β-sheets were less stable than α-helices due to fewer intermolecular hydrogen bonds (Jackson & Mantsch, 1995; Segat et al., 2014), and the β-turns and random coils were associated with protein unfolding, dissociation, and rearrangement (Xu et al., 2017). Therefore, according to these results, the increase in PUL caused gradual deformation or unfolding of α-helices in the secondary structure of COL. As a result, the tight and ordered α-helices were no longer stable and partially converted to less stable β-sheets and looser random coil structures. These results corresponded to previous studies to obtain spinnable materials, which indicated that the proteins should be unfolded, and random coils need to be generated for electrospinning (Rostami et al., 2019).

3.5. CD

The CD spectra were used to evaluate the fraction of the triple helical structure present of COL in the COL/PUL ultra-thin fibers. FDC showed the typical sinusoidal CD spectra of natural COL, with a deep negative peak at 198 nm and a small positive peak at 220 nm (Fiorani et al., 2014). The CD spectra of FDC, DNC, and CP1–6 are shown in Fig. 5A, expressed as the mean molar residual ellipticity. The denaturation of COL or disruption of its triple helix structure would cause the intensity of the positive peak at 221 nm and the negative peak at 198 nm to weaken. When the COL was completely denatured, the positive peak would completely disappear (Liu et al., 2010). It was clear that DNC showed complete disappearance of the positive peak and negative peaks with lower intensity, which was consistent with the literature. The lower ellipticity of CP1–6 compared to FDC on the positive peak indicated that the triple helix structure of CP1–6 was partially disrupted. The retained triple helical fractions of COL in CP1–6 were calculated using Eq. (3), with values of 44.92 %, 41.66 %, 41.24 %, 38.84 %, 39.11 %, and 36.69 %. The retained triple helix fractions of CP1–6 were higher than those of acetic acid-spun COL fibers (40 % v/v, acetic acid) (28.89 %) and HFP-spun COL fibers (12.51 %) (Liu et al., 2010), COL nanofibers prepared with trifluoroethanol (16 %) and AcOH/ddH_2O (20/80, v/v) (18 %) (Fiorani et al., 2014), and HFIP-prepared electrospun collagen fibers (Li et al., 2019). These results indicated that COL-based fibers prepared with 0.4 M acetic acid as a solvent resulted in a lower degree of protein denaturation.

3.6. Porosity analysis

The porosity of the nanofibers was affected mainly by the diameter and morphology of the fibers (Tort et al., 2017). The COL/PUL ultra-thin fiber porosity obtained from the SEM images at 16000 × magnification is shown in Fig. 5B. As previously reported, for the electrospun fibers, a reduction in fiber diameter led to an increase in porosity (Rad, Mokhtari, & Abbasi, 2018). Although CP1 and CP2 had smaller fiber diameters than CP3 (Fig. 3), they had lower porosity than CP3 (66.59 ± 1.07 %) due to the presence of fiber bundles. The porosities obtained for CP3–6 were 66.59 ± 1.07 %, 59.49 ± 1.57 %, 51.81 ± 0.11 % and 47.90 ± 2.23 %. With the increasing proportion of PUL, the porosity of the ultra-thin fibers decreased ($p < 0.05$), which could be attributed to an increase in fiber diameter and the formation of fiber bundles. In tissue

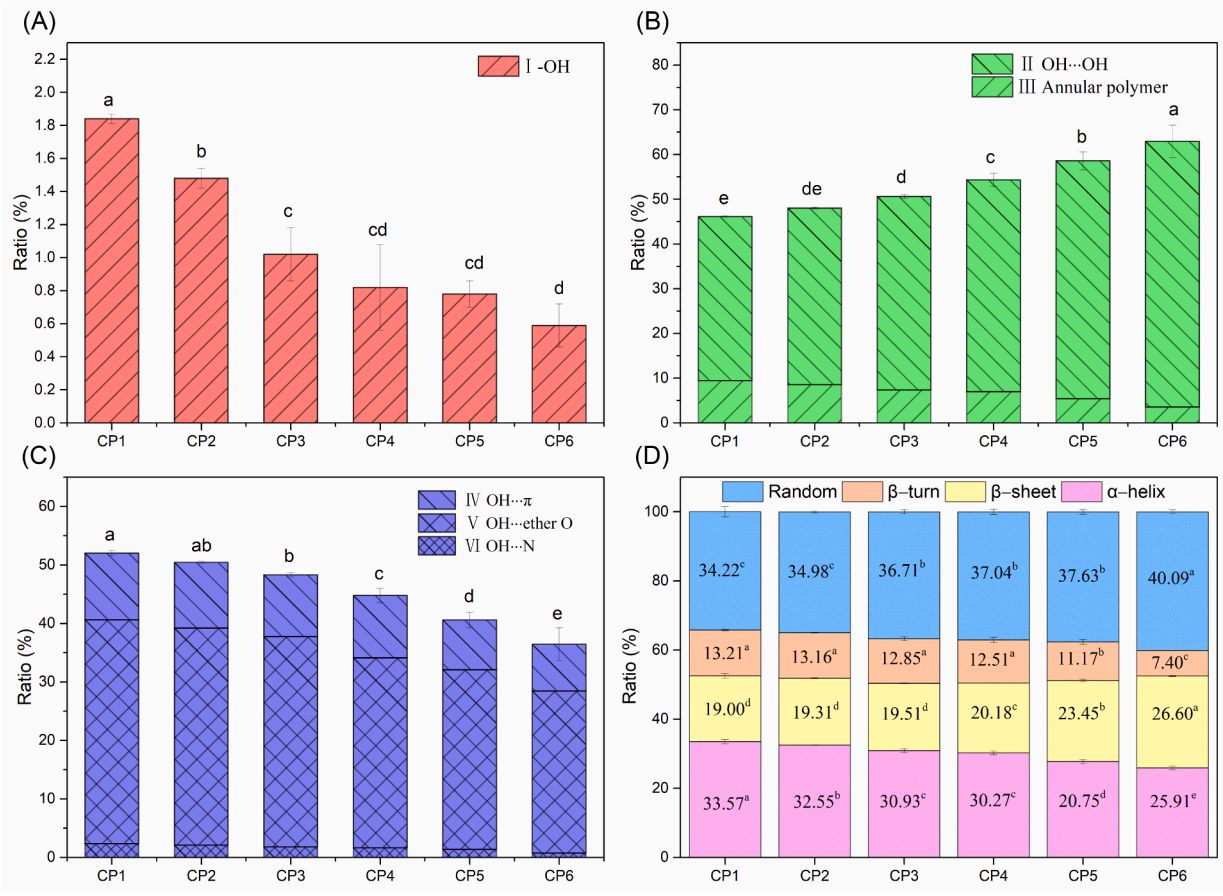

Fig. 4. Gaussian curve-fitting resulted of infrared spectrum of COL/PUL ultra-thin fibers. (A–C) –OH region (3800–3000 cm^{-1}), (D) amide I band (1700–1600 cm^{-1}).

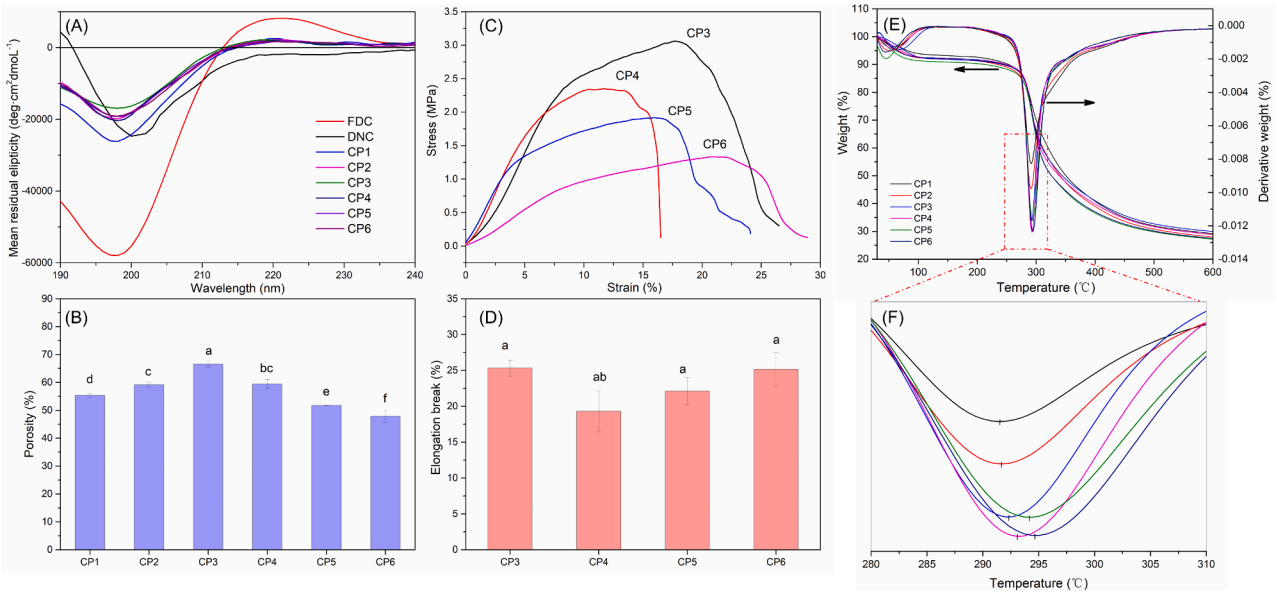

Fig. 5. Properties of COL/PUL ultra-thin fibers. (A) CD, (B) Stress–strain curves, (C) elongation-at-break, (D) Porosity, (E) TGA curves, (F) DTG curve.

engineering, fibers must have high porosity to imitate ECM and create a suitable environment for cell attachment, migration, and proliferation (Tort et al., 2017), with preferred fiber porosity for cell penetration in the range of 60 %–90 % (Rad et al., 2018). In this study, the porosities of CP3 were in the range of cell penetration, so they have the potential to be used in the field of biomedical materials.

3.7. *Mechanical property analysis*

Packaging materials must have sufficient mechanical strength and extensibility to withstand external stresses (Shah et al., 2023). Under the same electrospun requirements and times, CP1 and CP2 were deemed too thin for measurement. We found that the collection plates of CP1 and

CP2 had many rough holes in the fiber appearance, which could be the result of weaker entanglement leading to the inability to shape the Taylor cone plume. This led to the accumulation of thinner fibers on the collection plate. In this study, the tensile strengths of CP3–6 were 3.10 ± 0.16, 2.33 ± 0.20, 1.98 ± 0.13 and 1.33 ± 0.17 MPa (Fig. 5C), and the elongation-at-break values were 25.33 ± 1.10 %, 19.33 ± 2.85 %, 22.13 ± 1.88 % and 25.18 ± 2.31 % (Fig. 5D), respectively. The greater tensile strength of CP3 was likely related to its smooth morphology and smaller average fiber diameter, which could resist the applied forces by distributing the stress more evenly, resulting in greater elongation-at-break. The lower tensile strengths of CP5 and CP6 were possibly due to the appearance of fiber bundles in the ultra-thin fibers, which made them unevenly stressed. For CP4–6, the increase in elongation-at-break may be attributed to increased PUL content, making the obtained ultra-thin fibers have greater flexibility. In this study, the COL/PUL ultra-thin fibers had a tensile strength in the range of 1.33–3.10 MPa, suggesting that these ultra-thin fibers have excellent potential to be used in packaging materials and tissue engineering (Tort et al., 2017).

3.8. Thermal stability analysis

The thermal stability of the COL/PUL ultra-thin fibers was measured by TGA. The TGA and derivative thermogravimetric (DTG) curves for the COL/PUL ultra-thin fibers are shown in Fig. 5(E–F). According to Fig. 5E, the COL/PUL ultra-thin fibers exhibited two principal stages of thermal weight loss. The first thermal weight loss stage occurred between 30 °C and 100 °C, which was attributed to the vaporisation of residual moisture in the ultra-thin fibers. The second major weight loss occurred between 270 °C and 320 °C, which could be attributed to the degradation of the ultra-thin fibers (Zhang et al., 2018). Fig. 5F shows that the centre of the peaks shifted to a higher temperature as the ratio of PUL in COL/PUL increased (291.50 °C, 291.67 °C, 292.33 °C, 293.17 °C, 294.17 °C, and 294.67 °C), suggesting that an increase in PUL content in the COL/PUL system led to slightly increased thermal stability of the resulting ultra-thin fibers.

4. Conclusions

In this study, COL/PUL ultra-thin fibers were successfully fabricated by electrospinning using 0.4 M acetic acid as a solvent. The introduction of PUL was favourable for increasing the intermolecular entanglement of COL and PUL, which improved the spinnability of COL, and achieved the transformation of ultra-thin fiber morphology from spindle-like to smooth. With the spinnability of the COL electrospun solution increased, the proteins partially unfolded, and over 36 % of the triple helix fraction was retained. The FT-IR analysis results showed that with the inclusion of PUL, COL/PUL ultra-thin fibers tended to form intramolecular hydrogen bonds through broken intermolecular hydrogen bonds. In addition, secondary structure analysis showed that COL gradually unfolded, with the α-helices and β-turns structure gradually transforming into the β-sheets and random coil structure. Furthermore, the tensile strength and elongation-at-break of the ultra-thin fibers were related to the diameter and morphology. Smooth, defect-free and small-diameter ultra-thin fibers exhibited outstanding mechanical strength and elongation-at-break. Overall, this study successfully prepared COL/PUL ultra-thin fibers without toxic solvents, and the interaction between COL and PUL molecules underlying the improved spinnability was investigated, offering useful information for the development of food COL-based fibers.

This work was supported by the National Natural Science Foundation of China [grant numbers 42076120, 41676129, 41106149]; the Scientific Research Foundation of the Third Institute of Oceanography, SOA [grant numbers 2019010]; and the Marine Economic Innovation & Development Project of Beihai [grant numbers Bhsfs008].

CRediT authorship contribution statement

Junde Chen: Writing – review & editing, Funding acquisition. **Jianying Li:** Data curation, Software. **Yushuang Li:** Software. **Sijia Wu:** Software, Writing – original draft.

Declaration of competing interest

The authors declare that they have no known competing financial interests or personal relationships that could have appeared to influence the work reported in this paper.

Data availability

Data will be made available on request.

Appendix A. Supplementary data

Supplementary data to this article can be found online at https://doi.org/10.1016/j.fochx.2024.101138.

References

Aceituno-Medina, M., Mendoza, S., Lagaron, J. M., & Lopez-Rubio, A. (2013). Development and characterization of food-grade electrospun fibers from amaranth protein and pullulan blends. *Food Research International, 54*(1), 667–674. https://doi.org/10.1016/j.foodres.2013.07.055

Bhattarai, R. S., Bachu, R. D., Boddu, S. H. S., & Bhaduri, S. (2019). Biomedical Applications of Electrospun Nanofibers: Drug and Nanoparticle Delivery. *Pharmaceutics*, *11*(1), 5. https://doi.or g/10.3390/pharmaceutics11010005.

Blackstone, B. N., Gallentine, S. C., & Powell, H. M. (2021). Collagen-based electrospun materials for tissue engineering: A systematic review. *Bioengineering, 8*(3), 39. https://doi.org/10.3390/bioengineering8030039

Chen, J. D., Li, J. Y., Li, Z. B., Yi, R. Z., Shi, S. J., Wu, K. Y., Li, Y. S., & Wu, S. J. (2018). Physicochemical and functional properties of type I collagens in red stingray (dasyatis akajei) skin. *Marine Drugs, 17*(10), 558. https://doi.org/10.3390/md17100558

Colín-Orozco, J., Zapata-Torres, M., Rodríguez-Gattorno, G., & Pedroza-Isla, R. (2015). Properties of poly (ethylene oxide)/whey protein isolate nanofibers prepared by electrospinning. *Food Biophysics, 10*(2), 134–144. https://doi.org/10.1007/s11483-014-9372-1

Drosou, C., Krokida, M., & Biliaderis, C. G. (2018). Composite pullulan-whey protein nanofibers made by electrospinning: Impact of process parameters on fiber morphology and physical properties. *Food Hydrocolloids, 77*, 726–735. https://doi.org/10.1016/j.foodhyd.2017.11.014

Fiorani, A., Gualandi, C., Panseri, S., Montesi, M., Marcacci, M., Focarete, M. L., & Bigi, A. (2014). Comparative performance of collagen nanofibers electrospun from different solvents and stabilized by different crosslinkers. *Journal of Materials Science: Materials in Medicine, 25*, 2313–2321. https://doi.org/10.1007/s10856-014-5196-2

Guo, S. J., He, L. L., Yang, R. Q., Chen, B. Y., Xie, X. D., Jiang, B., Tian, W. D., & Ding, Y. (2020). Enhanced effects of electrospun collagen-chitosan nanofiber membranes on guided bone regeneration. *Journal of Biomater Science, Polymer Edition, 31*(2), 155–168. https://doi.org/10.1080/09205063.2019.1680927

Han, S. O., Youk, J. H., Min, K. D., Kang, Y. O., & Park, W. H. (2008). Electrospinning of cellulose acetate nanofibers using a mixed solvent of acetic acid/water: Effects of solvent composition on the fiber diameter. *Materials Letters, 62*(4–5), 759–762. https://doi.org/10.1016/j.matlet.20 07.06.059

Horuz, T. I., & Belibagli, K. B. (2018). Nanoencapsulation by electrospinning to improve stability and water solubility of carotenoids extracted from tomato peels. *Food Chemistry, 268*, 86–93. https://doi.org/10.1016/j.foodchem.2018.06.017

Irastorza, A., Zarandona, I., Andonegi, M., Guerrero, P., & Caba, K. (2021). The versatility of collagen and chitosan: From food to biomedical applications. *Food Hydrocolloids, 116*, Article 106633. https://doi.org/10.1016/j.foodhyd.2021.106633

Jackson, M., & Mantsch, H. H. (1995). The use and misuse of FTIR spectroscopy in the determination of protein structure. *Critical Reviews in Biochemistry and Molecular Biology, 30*(2), 95–120. https://doi.org/10.3109/10409239509085140

Jafari, H., Lista, A., Siekapen, M. M., Ghaffari-Bohlouli, P., Nie, L., Alimoradi, H., & Shavandi, A. (2020). Fish collagen: Extraction, characterization, and applications for biomaterials engineering. *Polymers, 12*(10), 2230. https://doi.org/10.3390/polym12102230

Jia, W. B., Li, M., Liu, L. L., Zhou, H., Liu, X. K., Gu, G. F., Xiao, M., & Chen, Z. G. (2021). Fabrication and assessment of chondroitin sulfate-modified collagen nanofibers for small-diameter vascular tissue engineering applications. *Carbohydrate Polymers, 257*, Article 117573. https://doi.org/10.1016/j.carbpol.2020.117573

Jia, X. W., Qin, Z. Y., Xu, J. X., Kong, B. H., Liu, Q., & Wang, H. (2020). Preparation and characterization of pea protein isolate-pullulan blend electrospun nanofiber films. *International Journal of Biological Macromolecules, 157*, 641–647. https://doi.org/10.1016/j.ijbiomac. 2019.11.216

Kutzli, I., Gibis, M., Baier, S. K., & Weiss, J. (2019). Electrospinning of whey and soy protein mixed with maltodextrin – Influence of protein type and ratio on the production and morphology of fibers. *Food Hydrocolloids, 93*, 206–214. https://doi.org/10.1016/j.foodhyd.2019.02.028

Laemmli, U. K. (1970). Cleavage of structural proteins during the assembly of the head of bacteriophage T4. *Nature, 227*(5259), 680–685. https://doi.org/10.1038/227680a0

Li, D. S., Gao, Y. L., Wang, Y. Z., Yang, X. P., He, C. L., Zhu, M. F., Zhang, S. M., & Mo, X. M. (2019). Evaluation of biocompatibility and immunogenicity of micro/nanofiber materials based on tilapia skin collagen. *Journal of Biomaterials Applications, 33*(8), 1118–1127. https://doi.org/10.1177/0885328218820180

Liu, H., Wang, Z. Y., Suleman, R., Shen, Q. W., & Zhang, D. Q. (2019). Effect of protein thermal stability and protein secondary structure on the roasted mutton texture and colour from different cuts. *Meat Science, 156*, 52–58. https://doi.org/10.1016/j.meatsci.2019.05.014

Liu, T., Teng, W. K., Chan, B. P., & Chew, S. Y. (2010). Photochemical crosslinked electrospun collagen nanofibers: Synthesis, characterization and neural stem cell interactions. *Journal of Biomedical Materials Research Part A, 95*, 276–282. https://doi.org/10.1002/jbm.a.32831

Ma, Y. H., Teng, A. G., Zhang, K. X., Zhang, K., Zhao, H. Y., Duan, S. M., Li, S. Z., Guo, Y., & Wang, W. H. (2020). A top-down approach to improve collagen film's performance: The comparisons of macro, micro and nano sized fibers. *Food Chemistry, 309*, Article 125624. https://doi.org/10.1016/j.foodchem.2019.125624

Manning-Benson, S., Bain, C. D., Darton, R. C., Sharpe, D., Eastoe, J., & Reynolds, P. (1997). Invasive and noninvasive measurements of dynamic surface tensions. *Langmuir, 13*(22), 5808–5810. https://doi.org/10.1021/la970457v

Miele, D., Catenacci, L., Rossi, S., Sandri, G., Sorrenti, M., Terzi, A., Giannini, C., Riva, F., Ferrari, F., Caramella, C., & Bonferoni, M. C. (2020). Collagen/PCL Nanofibers Electrospun in Green Solvent by DOE Assisted Process. An Insight into Collagen Contribution. *Materials, 23*(21), 4698. https://doi.org/10.3390/ma13214698

Mobika, J., Rajkumar, M., Sibi, S. L., & Priya, V. N. (2021). Investigation on hydrogen bonds and conformational changes in protein/polysaccharide/ceramic based tri-component system. *Spectrochimica Acta Part A: Molecular and Biomolecular Spectroscopy, 244*, Article 118836. https://doi.org/10.1016/j.saa.2020.118836

Mohammadi, M. A., Ramazani, S., Rostami, M., Raeisi, M., Tabibiazar, M., & Ghorbani, M. (2019). Fabrication of food-grade nanofibers of whey protein Isolate-Guar gum using the electrospinning method. *Food Hydrocolloids, 90*, 99–104. https://doi.org/10.1016/j.foodhy d.2018.12.010

Mouzouvi, C. R. A., Umerska, A., Bigot, A. K., & Saulnier, P. (2017). Surface active properties of lipid nanocapsules. *Plos One, 12*(8), e0179211.

Rad, Z. P., Mokhtari, J., & Abbasi, M. (2018). Fabrication and characterization of PCL/zein/gum arabic electrospun nanocomposite scaffold for skin tissue engineering. *Material Science and Engineering C, 93*, 356–366. https://doi.org/10.1016/j.msec.2018.08.010

Rostami, M., Yousefi, M., Khezerlou, A., Mohammadi, M. A., & Jafari, S. M. (2019). Application of different biopolymers for nanoencapsulation of antioxidants via electrohydrodynamic processes. *Food Hydrocolloids, 97*, Article 105170. https://doi.org/10.1016/j.foodhyd.2019.06.015

Segat, A., Misra, N. N., Fabbro, A., Buchini, F., Lippe, G., Cullen, P. J., & Innocente, N. (2014). Effects of ozone processing on chemical, structural and functional properties of whey protein isolate. *Food Research International, 66*, 365–372. https://doi.org/10.1016/j.foodres.201 4.10.002

Shah, Y. A., Bhatia, S., Al-Harrasi, A., Afzaal, M., Saeed, F., Anwer, M. K., Khan, M. R., Jawad, M., Akram, N., & Faisal, Z. (2023). Mechanical properties of protein-based food packaging materials. *Polymers, 15*(7), 1724. https://doi.org/10.3390/polym15071724

Stie, M. B., Jones, M., Sorensen, H. O., Jacobsen, J., Chronakis, I. S., & Nielsen, H. M. (2019). Acids 'generally recognized as safe' affect morphology and biocompatibility of electrospun chitosan/polyethylene oxide nanofibers. *Carbohydrate Polymers, 215*, 253–262. https://doi.org/10.1016/j.carbpol.2019.03.061

Tort, S., Acartürk, F., & Besikci, A. (2017). Evaluation of three-layered doxycycline-collagen loaded nanofiber wound dressing. *International Journal of Pharmaceutics, 529*, 642–653. https://doi.org/10.1016/j.ijpharm.2017.07.027

Vu, T. H. N., Morozkina, T. N., Uspenskaya, M. V., & Olekhnovich, R. O. (2022, December). *Fabrication of Polyvinyl Alcohol Nanofibers for the Delivery of Biologically Active Molecules*. IEEE-EMBS Conference on Biomedical Engineering and Sciences, Kuala Lumpur, MAS. 10.1109/IECBES 54088.2022.10079434.

Wang, Q. Q., Nandgaonkar, A. G., Cui, J., Huang, F. L., Krause, W. E., Lucia, L. A., & Wei, Q. F. (2014). Atom efficient thermal and photocuring combined treatments for the synthesis of novel eco-friendly grid-like zein nanofibres. *RSC Advances, 4*(106), 61573–61579. 10.10339/c4ra11792a.

Xiao, Q., & Lim, L. T. (2018). Pullulan-alginate fibers produced using free surface electrospinning. *International Journal of Biological Macromolecules, 12*, 809–817. https://doi.org/10.1016/j.ijbi omac.2018.02.005

Xu, J., Chen, Z. J., Han, D., Li, Y. Y., Sun, X. T., Wang, Z. J., & Jin, H. (2017). Structural and Functional Properties Changes of -Conglycinin Exposed to Hydroxyl Radical-Generating Systems. *Molecules, 22*(11), 1893. https://doi.org/10.3390/molecules22111893

Zeugolis, D. I., Khew, S. T., Yew, E. S., Ekaputra, A. K., Tong, Y. W., Yung, L.-Y. L., Hutmacher, D. W., Sheppard, C., & Raghunath, M. (2008). Electro-spinning of pure collagen nano-fibres - Just an expensive way to make gelatin? *Biomaterials, 29*(15), 2293–2305. 10.1016 /j.biomaterials.2008.02.009.

Zhang, R., Guo, J., Liu, Y. F., Chen, S., Zhang, S., & Yu, Y. (2018). Effects of sodium salt types on the intermolecular interaction of sodium alginate/antarctic krill protein composite fibers. *Carbohydrate Polymers, 189*, 72–78. https://doi.org/10.1016/j.carbpol.2018.02.013